communications materials

A Nature Portfolio journal

Article

https://doi.org/10.1038/s43246-026-01109-w

Universal method for polyvalent ions' redox state quantification in inorganic materials down to trace concentrations

Alexis Duval [1] ✉, Nadja Greiner-Mai[2], Franziska Scheffler[1,2], Oksana Smirnova[1] & Lothar Wondraczek [1,2] ✉

The oxidation state control of polyvalent cations within materials is a pivotal determinant of their macroscopic properties and practical functionalities, from persistent and stress-stimulated luminescence, to energy storage and photocatalytic activity. Nonetheless, the resulting redox state is highly sensitive to synthetic conditions, and quantifying techniques aimed at its determination—while of the highest importance—remain constrained by practical challenges. In the present work, two simple and accessible wet-chemical methods for quantifying oxidizing and reductive species, employing basic and easy-to-handle glassware and reagents, are introduced to address this issue. After validation on analytical standards encompassing diverse chemistries, they are applied to concrete off-stoichiometry materials of relevance—whether amorphous or crystalline—involving various redox couples and species, from highly reductive (Eu^{2+}, Ti^{3+}) to highly oxidizing (Ce^{4+}, Tb^{4+}). The roles of the host composition and processing conditions in altering the redox equilibria are discussed, and the obtained results are reinforced by the use of complementary analytical techniques. Multiple perspectives are emphasized, including the identification and resolution of the local environments and distributions of polyvalent cations, the isolation of high-valence species, and the provision of key insights into multifaceted phenomena for the design of advanced materials.

Material functionality and performance are defined by an ensemble of attributes, including chemical composition, microstructural architecture, and defect physics. Within this context, the redox state—i.e., the relative fraction of constituting polyvalent cations—stands out as a decisive factor, exerting a profound influence on both local structural features and macroscopic properties[1,2]. Indeed, trace amounts of one species can drastically alter the viscosity, demixing, or optical behavior in glasses and melts, but also introduce unique functionalities within ceramics, from persistent luminescence to magnetic response[3–6]. Nevertheless, methodological constraints continue to hinder its accurate quantification, thereby limiting a comprehensive understanding of its full potential[7–10]. In essence, precisely controlling the fractions of polyvalent cations allows for achieving desired material response and performances—such as electrical conductivity, or stress-stimulated luminescence—for targeted technologies and uses (photocatalytic activity, high stimulus responsiveness, smart windows and displays)[2,11–14].

This equilibrium is extremely sensitive to the synthesis parameters—whether temperature, environment (oxygen fugacity, reducing agents), or equilibration time, where reductive (oxidizing) conditions obviously favor lower (upper) oxidation states—but also to secondary processing (irradiation with X-rays or UV light)[15–20]. Moreover, large optical basicities, reflecting the electron-donating capacity of the matrix, promote the oxidation of polyvalent cations[21–27], enabling access to uncommon oxidation states in solid-state chemistry (Fe^{4+}, Mn^{6+})[22,27,28]. Yet, quantifying the interplay between synthesis temperature, oxygen fugacity, and optical basicity on the final redox state is particularly intricate. Attempts at developing predictive models employing model compositions and redox couples (Eu^{3+}/Eu^{2+}, Ce^{4+}/Ce^{3+}) involved experiment-heavy approaches, where the parameter ranges still remained limited[22,29–31].

Although essential, quantitative determinations are challenging and curiously often overlooked, relying on techniques with severe limitations: (i) restricted accessibility (X-ray absorption near-edge structure XANES, extended X-ray absorption fine structure EXAFS, voltammetry), (ii) inertness of active species (Mössbauer spectroscopy, optical absorption spectroscopy, magnetometry, photoluminescence spectroscopy), (iii) the necessity of extensive standardization (electron spin resonance ESR, Raman

[1]Otto Schott Institute of Materials Research, Friedrich Schiller University Jena, Jena, Germany. [2]Center for Energy and Environmental Chemistry—CEEC, Friedrich Schiller University Jena, Jena, Germany. ✉e-mail: alexis.duval@uni-jena.de; lothar.wondraczek@uni-jena.de

spectroscopy, impedance spectroscopy), or (iv) the risk of altering the redox state during measurement (X-ray photoelectron spectroscopy XPS)[2,7–11,30,32–34].

Wet chemistry emerges as the most suitable approach, combining accessibility, high precision, and sensitivity to all redox-active species, irrespective of their matrix, and without requiring prior standardization. However, existing methods face limitations that prevent their ubiquitous use, lacking precision, generalization, or sustainability. In particular, the reported techniques (i) mostly considered solely mildly oxidizing or reductive species (Fe^{3+}, Cu^{+}), (ii) typically involved complex experimental conditions (protective atmosphere) and hazardous reagents and solvents ($FeCl_3$, NH_4VO_3, OsO_4 catalyst, HF, HNO_3), and (iii) lacked standardization and universality, with methodologies varying significantly amongst studies[9,18,35–40].

In this work, we present two unified methods—both potentiometric and colorimetric—for promptly quantifying the redox state of inorganic materials, even at trace concentrations of active species, namely QOS for the quantification of oxidizing species, and QRS for the quantification of reductive species. The general framework involves first the sample dissolution in the presence of quantitatively defined reactive species (I^-, Fe^{3+}), followed by titration of the reaction products (I_2, Fe^{2+}) to ultimately derive the materials' redox states based on their chemical formula. Unlike the above-mentioned techniques, the proposed approaches require only minimal sample mass and basic facilities, employing readily available, cost-effective, and safe reagents, without the need for prior sample preparation. Following validation using analytical standards and complementary optical absorption spectroscopy, they are applied to model multi-component and off-stoichiometry materials, whether amorphous or crystalline, encompassing diverse chemistries, synthesis conditions, and optical basicities. Specific and compounded cases—including mixed-anion matrices, three coexisting oxidation states, and mixed redox couples—are addressed, with the findings interpreted in the light of existing literature. Perspectives for advancing material design and deepening the comprehension of complex phenomena through better-defined composition-structure-property relationships are discussed.

Results

Methodology formulation

Quantification of oxidizing species (QOS). In 1946, Barthauer and Pearce developed a wet chemistry method known as the "active-oxygen determination" to quantify the proportions of tetravalent rare-earth (RE) ions in precursor oxides, which are especially scarce in solid-state, molecular, and aqueous chemistries[41,42]. In essence, it involved dissolving RE^{4+}-bearing compounds within solutions containing reactive agents (I^-) followed by titration of the reaction products (I_2 by $S_2O_3^{2-}$), effectively countering the tendency of RE^{4+} ions to promptly reduce in aqueous solutions ($E^\circ_{RE^{4+}/RE^{3+}} > E^\circ_{O_2/H_2O}$), following[43–45]:

$$2RE^{4+} + 2I^- \longrightarrow 2RE^{3+} + I_2 \qquad (E^\circ_{RE^{4+}/RE^{3+}} > E^\circ I_2/I^-) \tag{1}$$

$$2S_2O_3^{2-} + I_2 \longrightarrow S_4O_6^{2-} + 2I^- \qquad (E^\circ_{I_2/I^-} > E^\circ S_4O_6^{2-}/S_2O_3^{2-}) \tag{2}$$

Such electrochemical methods rely fundamentally on reduction-oxidation processes, in which, following sample dissolution, a multivalent cation of interest reacts with a chosen reductant or oxidant (e.g., RE^{4+} with I^-), driven by a favorable decrease in Gibbs free energy. These reactions can be regarded as complete when the difference in standard potentials is sufficiently large (e.g., $E^\circ_{RE^{4+}/RE^{3+}} - E^\circ_{I_2/I^-} > 0.24$ V, ensuring an equilibrium constant $K > 10^4$ for a one-electron transfer) and are not kinetically hindered. In a second time, and in a similar manner, the reaction products can be titrated (e.g., I_2 with $S_2O_3^{2-}$), thereby allowing deduction of the initial concentration of RE^{4+}. Such methods are thus applicable to any multivalent element (including transition metals, rare earths, and p-block elements), provided that: (i) no competing ions in the matrix react with the selected reagent (e.g., Al^{3+} from aluminates cannot react with I^-, owing to the small Al^{3+}/Al^0 standard potential of −1.677 V[43]), (ii) complete dissolution of the sample is achieved, and (iii) the initial quantities of all species are appropriately defined.

Although originally confined to stoichiometric rare-earth oxides, here we propose to extend and adapt this method to any material containing M^{y+} oxidizing species, provided that $E^\circ_{M^{y+}/M^{x+}} > E^\circ_{I_2/I^-}$. To illustrate this, let us consider a model material, $A_aB_bM_mZ_z$, where A, B, and M represent cations, with respective cationic fractions a, b, and m ($a + b + m = 100$ cat.%). Here, M is a multivalent cation (with possible valencies M^{y+} and M^{x+}, where $y > x$). The oxidized fraction f_{ox} can thus be defined as:

$$f_{ox} = \frac{[M^{y+}]}{[M^{y+}] + [M^{x+}]} \tag{3}$$

where $[M^{y+}]$ and $[M^{x+}]$ are the respective concentrations of each valency. At last, Z is an anion for which the value z is determined by the concentrations and valencies of each constituting ion i, generally termed v_i: $z = \frac{av_a + bv_B + m[v_{M^{x+}} + f_{ox}\cdot(v_{M^{y+}} - v_{M^{x+}})]}{v_Z}$. Accordingly, the formulation of the material can be represented using various conventions commonly adopted in materials science, ranging from atomic percent (at.%), weight percent (wt.%), to mole percent (mol.%), with the latter given by: $a\,A_{v_Z}Z_{v_A} - b\,B_{v_Z}Z_{v_B} - m\cdot f_{ox}\,M_{v_Z}Z_{v_{M^{y+}}} - m\cdot(1 - f_{ox})\,M_{v_Z}Z_{v_{M^{x+}}}$. First, the weight fraction $wt.\%_{M^{y+}}$ of oxidizing species M^{y+} can be quantified, such as:

$$wt.\%_{M^{y+}} = \frac{100 \cdot V_{eq} \cdot C_{S_2O_3^{2-}} \cdot M_M}{m_{sample} \cdot (v_{M^{y+}} - v_{M^{x+}})} \tag{4}$$

where V_{eq} is the equivalence volume, $C_{S_2O_3^{2-}}$ is the concentration of the titrating sodium thiosulfate solution, M_M is the molar mass of the multivalent element, and m_{sample} is the mass of dissolved model material. Then, the oxidized fraction f_{ox} can be deduced directly from its chemical formula, according to:

$$f_{ox} = wt.\%_{M^{y+}} \times \frac{\left[\frac{M_Z}{v_Z}(av_A + bv_B + mv_{M^{x+}}) + (aM_A + bM_B + mM_M)\right]}{\left[(100 \cdot mM_M) - \left(\frac{wt.\%_{M^{y+}} \cdot mM_Z \cdot (v_{M^{y+}} - v_{M^{x+}})}{v_Z}\right)\right]} \tag{5}$$

Quantification of reductive species (QRS). Building upon the QOS method, a parallel approach can be devised for quantifying reductive species (i.e., species prone to oxidation in aqueous media). In this method, ferric ions are used as reactive agents to oxidize M^{x+} ions (on the condition that $E^\circ_{Fe^{3+}/Fe^{2+}} > E^\circ_{M^{y+}/M^{x+}}$) and prevent their oxidation with the ambient atmosphere. The resulting reaction products are subsequently titrated (Fe^{2+} by Ce^{4+}). Taking Cu^+ as a representative example, the reactions write:

$$Fe^{3+} + Cu^+ \rightarrow Fe^{2+}Cu^{2+} \qquad \left(E^\circ_{Fe^{3+}/Fe^{2+}} > E^\circ_{Cu^{2+}/Cu^+}\right) \tag{6}$$

$$Fe^{2+} + Ce^{4+} \rightarrow Fe^{3+} + Ce^{3+} \qquad (E^\circ_{Ce^{4+}/Ce^{3+}} > E^\circ_{Fe^{3+}/Fe^{2+}}) \tag{7}$$

This methodology even allows for the determination of species whose standard potential lies outside the electrochemical window of water ($E^\circ_{M^{y+}/M^{x+}} < E^\circ_{H^+/H_2}$). The weight fraction $wt.\%_{M^{x+}}$ of reductive species M^{x+}, as well as the corresponding reduced fraction f_{red} can thus be quantified as:

$$wt.\%_{M^{x+}} = \frac{100 \cdot V_{eq} \cdot C_{Ce^{4+}} \cdot M_M}{m_{sample} \cdot (v_{M^{y+}} - v_{M^{x+}})} \tag{8}$$

$$f_{red} = 1 - f_{ox} = wt.\%_{M^{x+}} \times \frac{\left[\frac{M_Z}{v_Z}\left(av_A + bv_B + mv_{M^{y+}}\right) + \left(aM_A + bM_B + mM_M\right)\right]}{\left[\left(100 \cdot mM_M\right) + \left(\frac{wt.\%_{M^{x+}} \cdot mM_Z \cdot \left(v_{M^{y+}} - v_{M^{x+}}\right)}{v_Z}\right)\right]} \quad (9)$$

where $C_{Ce^{4+}}$ is the concentration of the titrating ceric sulfate solution.

The selection of the appropriate method is therefore determined by considering the standard potential and corresponding Pourbaix diagram of the species involved[46]: The QRS method is suitable for ionic species that are susceptible to oxidation in aqueous solutions ($E^{\circ}_{M^{y+}/M^{x+}} < 0.77$ V, e.g., Eu^{2+}, Cu^{+}, Sn^{2+}), whereas the QOS method is ideal for species that are prone to reduction ($E^{\circ}_{M^{y+}/M^{x+}} > 0.545$ V, e.g., Cr^{6+}, Ce^{4+}, Tb^{4+}). Together, they allow for the determination of the oxidized fraction of materials containing polyvalent cations, regardless of the standard potential of their redox couples (see Supplementary Fig. 1).

Presentation of the apparatus and validation of the methods

The versatile experimental apparatus designed for redox quantification is illustrated in Supplementary Fig. 2a. Comprising simple components (thus eliminating the need for commonly used platinum or Teflon containers) and operating without the need for a protective atmosphere, it is suitable for both The Quantification of Oxidizing Species (QOS) and Quantification of Reductive Species (QRS) wet chemistry methods. A condensed workflow chart summarizing the experimental procedure across various chemical matrices and redox couples is provided in Fig. 1, with the corresponding logic tree presented in Supplementary Fig. 1. A preconfigured calculation sheet (Supplementary Data 1), featuring two representative cases, is available in the Supplementary Information. Briefly, samples are dissolved in the presence of reactive agents (I^{-}, Fe^{3+}); following complete reaction with the active species, the reaction products (I_2, Fe^{2+}) are titrated (with $S_2O_3^{2-}$ or Ce^{4+}, respectively), therefore enabling, following blank determination (as presented in Supplementary Fig. 3a–f), the subsequent calculation of the material redox state. A typical redox quantification involves small quantities of samples and readily accessible non-hazardous reagents (from tens to hundreds of milligrams). An entire experiment, from sample dissolution to equivalence volume determination, is completed under 30 min at a total reagent cost at a few-euro scale, ensuring a methodology that is simple, non-toxic, rapid, environment-friendly, as well as resource- and cost-effective. Comparative workflow charts and tables, emphasizing the capabilities of the framework (e.g., combination of universality, accessibility, and sampling) relative to existing means of redox state quantification—be they spectroscopic or chemical—are provided in Supplementary Fig. 4 and Supplementary Table 1. Furthermore, the equivalence volumes, reflected by a pronounced color shift during titration (with or without an indicator, as shown in Supplementary Fig. 2b, c) can also be deduced using a complementary potentiometer, thereby enhancing the precision of the proposed methods, with analytical uncertainties (as detailed in the Supplementary Information, from Supplementary Equations (1) to (17), and integrated into the preconfigured calculation sheet) typically lying within 2–3% of the determined oxidized (or reduced) fraction.

Considering two model cases for the QOS and QRS methods (Pr_6O_{11} and Cu_2O, respectively), the measured potentials align with theoretical expectations derived from the Nernst equation, and the determined equivalence volumes—as well as the corresponding oxidized fractions—are in agreement with the expected redox states of the analytical standards (presented in Fig. 2a, b and Fig. 2c, respectively). Extending these methods to additional analytical standards of varying chemistries confirms their suitability to oxides, nitrides, and fluorides, enabling the probing of their redox state even when the corresponding standard potential lies beyond the electrochemical window of water (which extends from 0 to 1.23 V in acidic conditions). Repeated measurements on SnF_2 (as seen in Supplementary Fig. 5a, b) yield accuracy and precision values (following application of Supplementary Equations (18) to (21)) of 99.7 and 0.4%, in good agreement with the calculated expanded uncertainty (±1.7%), thereby confirming the method's reliability. While their applicability to other halides (chlorides, bromides) is anticipated based on the involved redox couples[43], the methods are found unsuitable for sulfides (as illustrated with the examples of FeS and Cu_2S in Supplementary Fig. 6a–d). This limitation arises from the wide range of concurrent redox reactions (with standard potentials ranging from 0.54 to −0.17 V) involving multiple sulfur species—which readily engage in side reactions with Fe^{3+} and I_2—therefore suggesting limited applicability to other chalcogenides. The agreement in deduced oxidized fractions using both methods for Fe-bearing standards further confirms their reliability and validity. Note that in cases of multi-component materials or small concentrations of active species, slight deviations from expected absolute

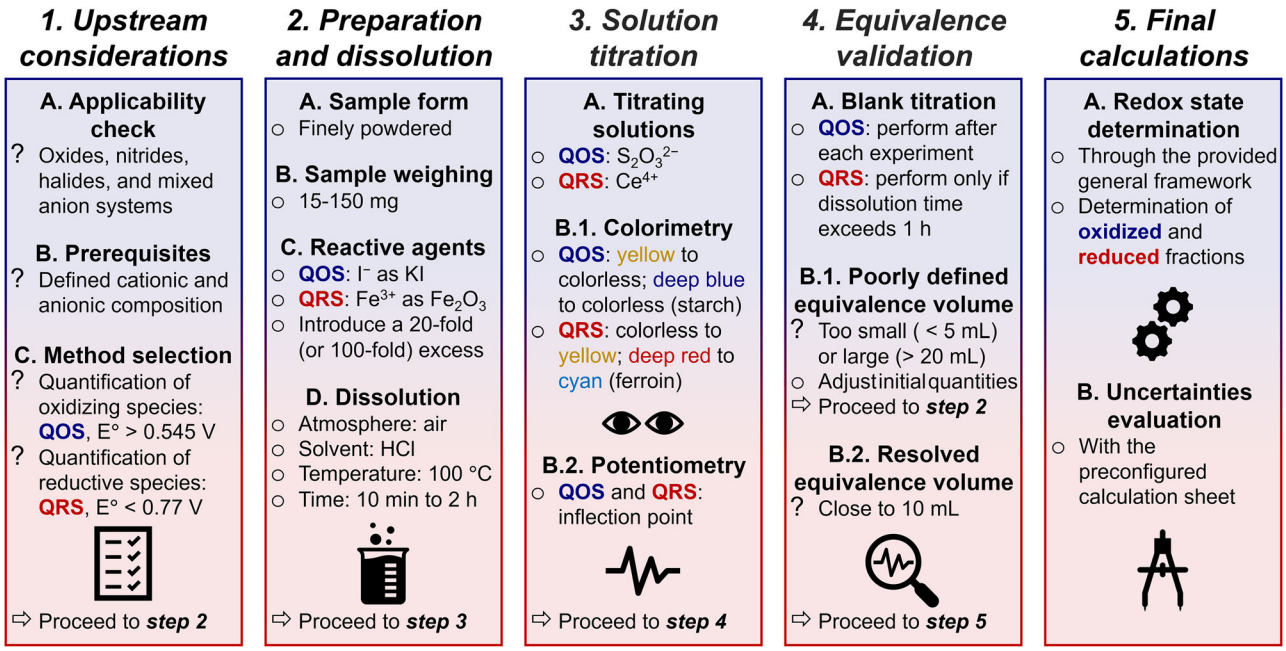

Fig. 1 | Conduction of redox state quantification experiments. Workflow chart for redox state quantification utilizing the QOS (Quantification of Oxidizing Species) and QRS (Quantification of Reductive Species) wet chemistry methods.

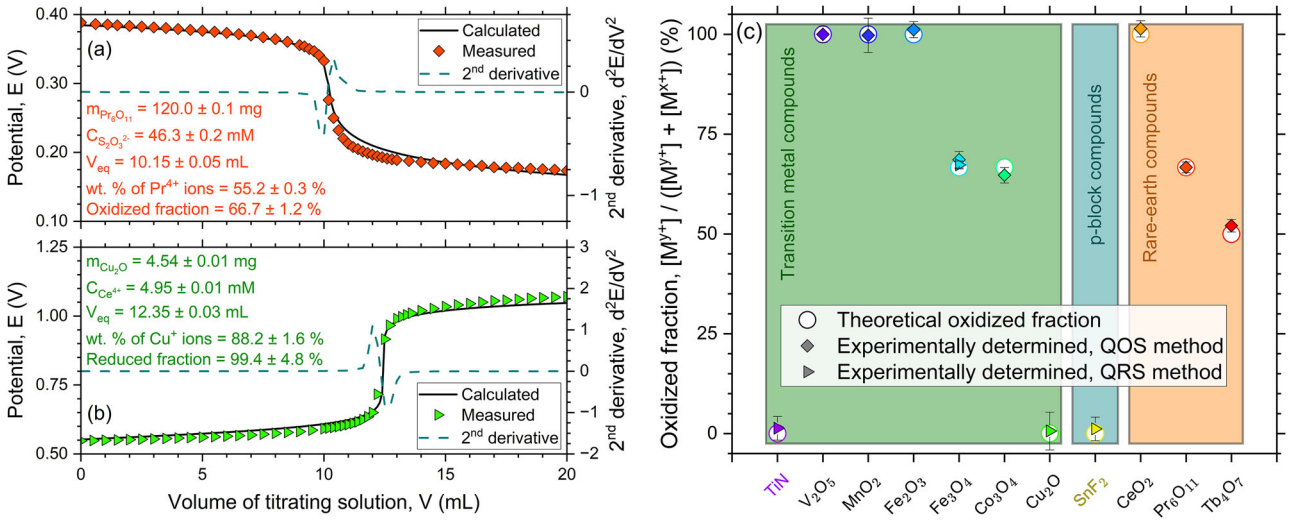

Fig. 2 | Presentation and validation of the QOS and QRS methods. Calculated and measured potentiometric curves with corresponding second derivatives for **a** Pr_6O_{11} (QOS method), and **b** Cu_2O (QRS method). **c** Expected and measured oxidized fractions for various analytical standards using the QOS and QRS methods.

potential values and associated shift sharpness can be observed. Therefore, normalizing the collected data and determining equivalence volumes through second derivative calculations is recommended for consistency (as shown in Supplementary Fig. 7a–c).

Nevertheless, certain limitations of the present methods must be acknowledged. These include (i) the occurrence of side reactions, which may lead to over- or underestimation of equivalence volumes, and (ii) the quantification of active species within corrosion-resistant matrices. The first limitation arises from either reactive elements within the material matrix (e.g., sulfur in sulfides, as previously discussed) or solvated oxidizing or reductive species (e.g., electrons in reduced CaO-Al_2O_3 glasses)[47]. Note, however, that large concentrations of such solvated species—e.g., exceeding the concentration of anionic vacancies accommodating the reduction of a multivalent element[6,48,49]—can only be achieved under extreme reducing conditions ($PO_2 \sim 10^{-24}$ atm), far from conventional Ar or N_2:H_2 atmospheres. The second limitation pertains to matrices in which hydrochloric acid does not achieve appreciable dissolution within reasonable experimental times, as in fused silica. The proposed adaptive framework remains valid in these cases, with dissolution conditions (acid type, temperature, and duration) modifiable to suit challenging samples. The adaptability of the approach, which will be presented later (see Eq. (11)), further allows extension to complex sample formulations by modifying Eqs. (5) and (9), including materials with atomic-level vacancy concentrations (when quantitatively determined, though even large vacancy concentrations alter the redox state by only ~1%) or materials containing solvent molecules (e.g., hydrates).

Application to off-stoichiometry materials

Following the validation of both methods using analytical standards, their application can now be extended to off-stoichiometry materials (e.g., glasses, glass-ceramics, doped ceramics). Hereafter, the results obtained (and shown in Supplementary Fig. 8a–e) from applying the QOS and QRS methods to multiple glasses and crystals, doped with varying types and concentrations of multivalent cations and synthesized under diverse conditions, are discussed. For instance, an oxidized fraction of 20.0 ± 0.6% is measured for a Ce-doped aluminosilicate glass, in agreement with XANES analyses reported in other works where an oxidized fraction of 19 ± 3% was determined for the same selected composition[18]. On the one hand, high oxidation states of manganese with characteristic photoluminescence properties were recently evidenced in glasses and crystals[27,50,51]. Using the QOS method, a high Mn^{5+} fraction of 78.9 ± 1.7% (i.e., a mean $v_{M^{y+}} - v_{M^{x+}}$ difference of 4.58–2 = 2.58 for f_{ox} = 100%) is obtained for a Mn-doped 68 Na_2O – 32 B_2O_3 glass (mol.%), whereas Mn^{5+} and Mn^{6+} fractions of 26.0 and 74.0 ± 1.6% respectively are identified in a Mn-doped 50 SiO_2 – 40 Cs_2O – 10 BaO glass (mol.%). On the other hand, the reduced fraction of Eu^{2+} in phosphors is rarely quantified, despite its critical consequences on their persistent luminescence and mechanoluminescence properties. By applying the QRS method, reduced fractions of 96.1 ± 1.9% and 91.0 ± 1.8% are determined for $Ba_4Si_6O_{16}$:Eu^{2+}, Ho^{3+} crystals (from ref. 52) and commercial $SrAl_2O_4$:Eu^{2+}, Dy^{3+}, respectively. These results align with the few existing ^{151}Eu Mössbauer spectroscopy analyses of Eu-doped oxides synthesized under similar conditions (N_2:H_2 atmosphere), where the Eu^{2+} fraction ranged from about 90–95%[53,54]. Both methods thus yield oxidized fractions consistent with other analytical techniques in but a single experiment, eliminating the need for sequential measurements (e.g., first determining the Fe^{2+} content before total Fe content in Fe-bearing materials) which are not only time- and resource-intensive but also unsuitable for specific species (Eu^{2+}, Tb^{4+}). Moreover, complete sample dissolution is confirmed even for SiO_2-rich compositions, as evidenced by the invariance of the measured oxidized (or reduced) fractions with respect to both sample mass and dissolution time (shown in Supplementary Fig. 91a, b). Yet, when non-negligible volatilization occurs during sample synthesis (e.g., K_2O, Rb_2O), appropriate preliminary measures must be undertaken to ensure the exact cationic composition is used for final calculations (energy dispersive X-ray analysis, EDX, electron microprobe analyzer EMPA). Using the NaB series as a representative example, major compound volatilization of ~5 mol.% would result in tolerable oxidized fraction misestimations of less than 5% of the measured value.

The logarithm of the reduced-to-oxidized species ratio R, $\log(R = [M^{x+}]/[M^{y+}])$, for various glass matrices and associated redox couples is plotted against the corresponding standard potential E° in aqueous solutions in Fig. 3a. The corresponding glass compositions and oxidized fractions are provided in Supplementary Table 2 and Supplementary Table 3, respectively. Over the investigated range, log(R) increases approximately linearly with E° irrespective of the glass matrix, though some discrepancies are observed and will be discussed in the following section. For conventional glasses with optical basicities (Λ_{th}) ranging from 0.50 to 0.65, comparable amounts of both species are typically observed when E° ranges from 0.3 to 2.0 V, whereas only small quantities (a few percent) of oxidizing (reductive) species are noted for larger (smaller) E°. Indeed, E° reflects the tendency of a chemical species to gain electrons. Although absolute values vary across glass-forming melt compositions, a systematic linear relationship between E° in aqueous solutions and E° in glass-forming melts was observed, supporting the use of E° in aqueous solutions as a representative parameter regardless of the host matrix[39]. It therefore plays a major role in redox state control, as a 1 V change in E° can substantially alter the oxidized

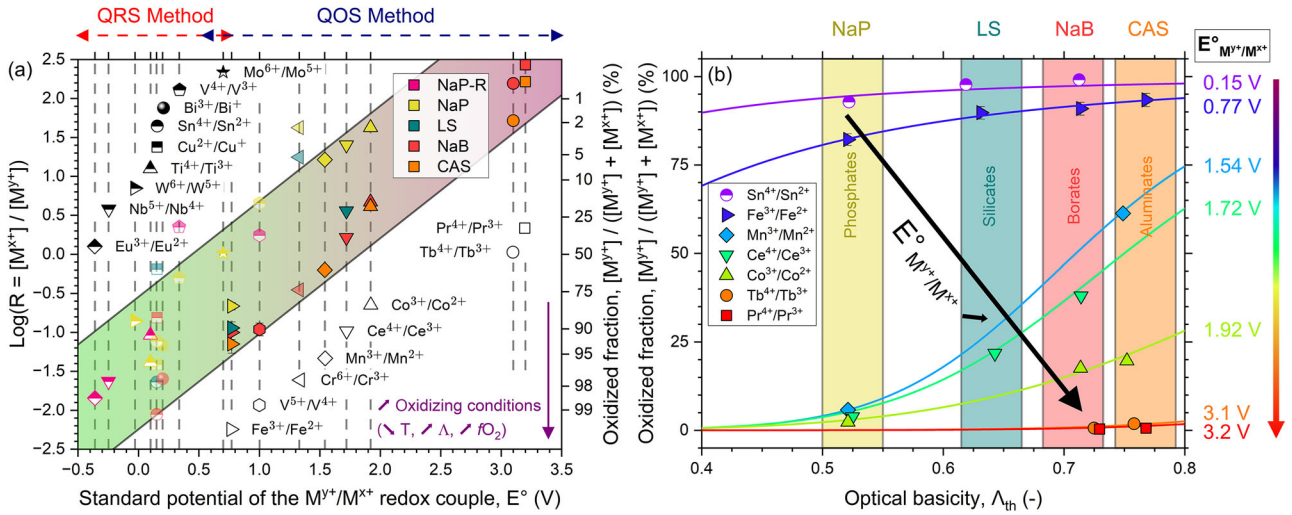

Fig. 3 | Polyvalent ions' redox state across representative glass families. **a** Logarithm of the reduced-to-oxidized species ratio, log(R), against the corresponding standard potential in aqueous solutions, $E^{\circ}_{M^{y+}/M^{x+}}$, for the investigated glass series. Oxidized fractions derived from the QRS method are represented by half-filled symbols, whereas those from the QOS method are indicated as filled symbols. Outliers (discussed in the main text) are depicted in lighter shades. E° values are taken from ref. 43, while estimated values of E° for the Tb^{4+}/Tb^{3+} and Pr^{4+}/Pr^{3+} redox couples are selected from ref. 73. **b** Oxidized fraction of several redox couples within glass matrices of varying optical basicities. Variations in matrix optical basicity resulting from the introduction of dopants are considered[23,25,26].

fractions by an order of magnitude. Likewise, variations in oxidizing conditions amongst the glass series—matrix optical basicity, synthesis temperature, and oxygen fugacity—result in similar shifts. This is demonstrated in Fig. 3b, where an exponential—or rather sigmoidal—increase in oxidized fraction is observed with increasing optical basicity (or increased mean cationic polarizability) of the host matrix (from phosphates to silicates, borates, and aluminates). This concurrent interplay highlights their collective importance in achieving desired redox states. As such, the present dataset provides a fundamental framework for the rational design of material formulations with tailored properties to meet targeted applications.

Certain deviations from strict linearity are attributed to intrinsic aspects of redox state physicochemistry. Specifically, (i) variations in redox equilibrium sensitivity of each redox couple to distinct oxidizing conditions (e.g., higher sensitivity to temperature variations than to changes in optical basicity)[29,30,34,55–58], (ii) the ubiquitous behavior of the Cu^{2+}/Cu^{+} redox couple, which, for a given temperature, demonstrates an opposite dependence on optical basicity with respect to other redox couples, as discussed in ref. 22, (iii) disproportionation reactions occurring when three or more oxidation states coexist in the system (e.g., $V^{5+}/V^{4+}/V^{3+}$)[27,35,39], and (iv) redox couples involving multi-electron transfer processes (e.g., Cr^{6+}/Cr^{3+}, Sn^{4+}/Sn^{2+}), where equilibrium constants and reduced fractions are inherently larger than in single-electron transfer reactions[22,35,39].

Looking at the limits of the investigated E° range, even highly oxidizing or reductive species (Tb^{4+}, Nb^{4+})—only achievable in large fractions through ultrafast laser irradiation, and often challenging to properly assess[17,59]—can be quantified in trace amounts using the proposed methods (as exemplified for Yb^{2+} and Pr^{4+} in Supplementary Fig. 10a–f). By extending the observed general trend to extreme values of E°, it is expected that a few tens of ppm of Nd^{4+} and Dy^{4+} (E° = 5.0 and 5.2 V, respectively) and a few hundreds of ppm of Sm^{2+} and Yb^{2+} (E° = −1.55 and −1.05 V, respectively) are present in conventional glasses, species that are observed as major components only in a limited number of crystals or under extreme conditions[42,43]. Where unusually high oxidation states were achieved in specific glass hosts (Ni^{3+}, Pb^{4+})[22,35], it is anticipated that combining (i) appropriate glass matrices with exceptionally large optical basicities (in TeO_2-rich compositions, or in particular in the Cs_2O – B_2O_3 chemical system, which can accommodate alkali concentrations up to 73 mol.% corresponding to a Λ_{th} of 0.95[60]) with (ii) extreme oxygen fugacities[16], could enable the attainment of previously unobtainable large fractions of highly oxidizing species (Cu^{3+}, Mn^{7+}), providing unique physicoelectrical properties and stimulus responsiveness (akin to these of Mn^{5+} and Mn^{6+})[27,42,50].

Standardization of complementary analytical techniques

Unlike other analytical techniques, the QOS and QRS wet-chemical methods can be applied to any active species even down to trace amounts, provided that (i) the electrode sensitivity is sufficient, and (ii) the sample fully dissolves during the experiment. As a matter of example, oxidized fractions in glasses with nominal Fe concentrations as low as 0.02 at.% (or 200 ppm) can be measured for the NaB and NaP series, respectively (see Fig. 4a). Where the oxidized fraction remains nearly independent of Fe concentration in the NaB series, it oppositely significantly increases from about 80–87% in the NaP series as the Fe concentration increases by over two orders of magnitude (from 0.02 to 4.0 at.%). This difference arises because the optical basicity of the NaB matrix is already very large relative to that of the NaP matrix (Λ_{th} = 0.71 and 0.52, respectively), indicative that further increase in optical basicity following Fe_2O_3 addition (Λ_{th} = 1.04) has but limited consequences on the final redox state[24].

In essence, these methods provide a reliable reference for standardizing other techniques (XANES, XPS, ESR, Raman spectroscopy), thereby overcoming their inherent inaccuracies in redox state quantification while harnessing their characteristic advantages (spatial resolution, selectivity toward specific active species, sensitivity to environment-dependent electronic transitions, and short to medium range structural order). The representative case of optical absorption spectroscopy is selected, for which the spectra of the NaP-Fe series are presented in Fig. 4b. They consist of three prominent absorption bands: (i) one at ~23,000 cm^{-1}, corresponding to the $^6A_1(S) \rightarrow {}^4T_2$ transition of Fe^{3+}, whereas (ii) two at ~9500 and ~5000 cm^{-1} are assigned to the $^5T_{2g}(D) \rightarrow {}^5E_g(D)$ and $^5E(D) \rightarrow {}^5T_2(D)$ transitions of Fe^{2+} in octahedral and tetrahedral coordination, respectively[2,61]. Using the determined oxidized fractions and thus the concentration of active species C, the molar extinction coefficient ε associated with each electronic transition can be derived from the measured absorption coefficient α (i.e., absorbance A divided by the sample thickness d) following Beer–Lambert's law. For Fe^{2+}-related transitions, this writes:

$$\alpha = \frac{A}{d} = \varepsilon \cdot C = \varepsilon \cdot \frac{10 \cdot \text{wt.}\%_{Fe^{2+}} \times \rho}{M_{Fe}} \quad (10)$$

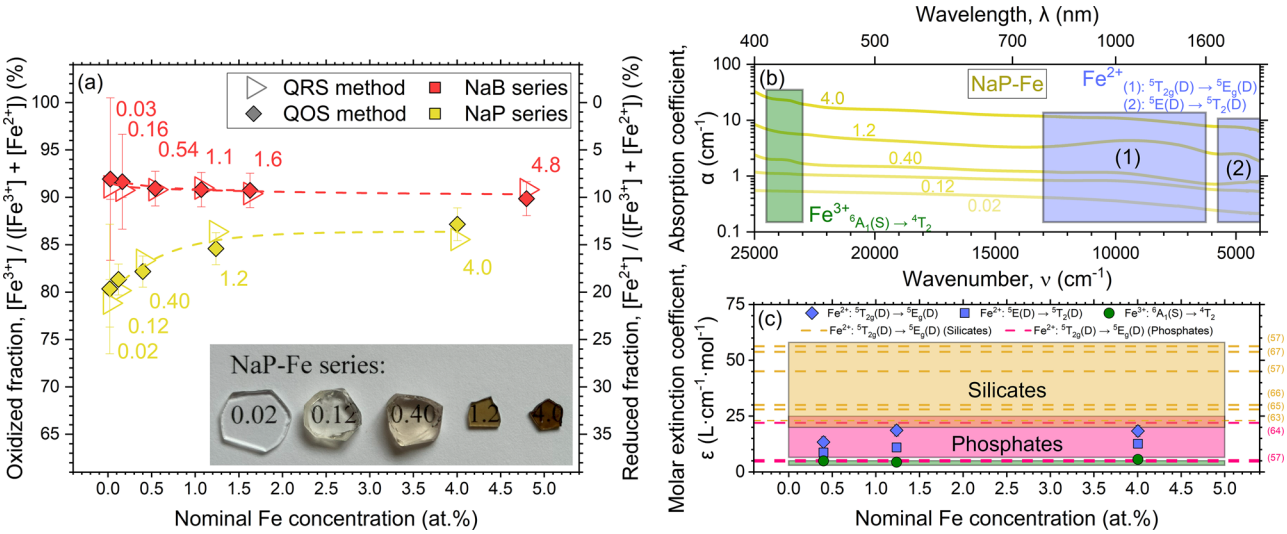

Fig. 4 | Calibration of Fe-related electronic transitions molar extinction coefficients between glass matrices. a Concentration-dependent oxidized fraction in Fe-bearing NaP and NaB glasses, determined utilizing the QOS (filled symbols) and QRS (open symbols) methods. The labels indicate the nominal Fe concentration in at.%. Photographs of the NaP-Fe samples are presented in the inset, highlighting the characteristic yellow to dark brown colors of Fe^{3+}-containing glasses[2,61]. **b** Optical absorption spectra of Fe-bearing NaP glasses with increasing nominal Fe concentration. Fe^{3+}- and Fe^{2+}-related electronic transitions are highlighted. Slight deviations at small wavenumbers are ascribed to residual water. **c** Concentration- and host-dependent molar extinction coefficients of Fe^{3+}- and Fe^{2+}-related electronic transitions. Values obtained in the present work are shown with symbols, and those from literature with dashes[2,55,57,61–68]. The absorption coefficient values for Fe-bearing NaP glasses at low doping levels are too small and therefore not indicated.

where ρ is the sample density. Although the measured ε are of the same order of magnitude as those reported for phosphate glasses, it is evident that preliminary redox state determinations—for instance using wet chemistry methods—are imperative before interpreting optical absorption spectra to avoid erroneous quantification (as shown in Fig. 4c). On the one hand, non-linearity in Beer–Lambert's law is known to arise beyond a certain saturation threshold (as seen for instance for $\varepsilon(5T_{2g}\,(D) \rightarrow {}^5E_g\,(D))$[62]. On the other hand, the host matrix—and thus the ligand field strength—play a critical role, as reported ε values vary by more than one order of magnitude between silicate and phosphate glasses[2,55,57,61–68]. Ultimately, once the redox state is properly calibrated, optical absorption spectroscopy (and other spectroscopic techniques) effectively become powerful tools for probing in situ the local environment and distribution of active species (clustering, partitioning, first coordination sphere, bonding type), whether within glasses, ceramics, or glass-ceramics—aspects that remain partly unresolved and continue to stimulate numerous research endeavors[19,20,27,50,62,65].

Adaptation to specific cases

Although both the QOS and QRS methods are found suitable for crystalline and amorphous off-stoichiometry materials of various chemistries, there are a few intricate cases that require minor modifications due to the complexity of the considered systems, while keeping the general methodology valid and applicable. Among those cases are: (i) mixed anion matrices, (ii) three coexisting oxidation states, and (iii) mixed redox couples. For the former (e.g., oxynitrides, oxyfluorides), it is necessary to assess the anionic composition beforehand, typically through EMPA or using a Leco® analyzer. From there, the equations for determining f_{ox} and f_{red} are rearranged appropriately. For instance, if Z and Q represent anions with anionic fractions f_Z and f_Q (where $f_Z + f_Q = 1$), then the expression for f_{red} becomes:

$$f_{red} = wt.\%_{M^{x+}} \times \frac{\left\{\left[\left(\frac{f_Z M_Z}{v_Z} + \frac{f_Q M_Q}{v_Q}\right) \times \left(av_A + bv_B + mv_{M^{y+}}\right)\right] + \left[aM_A + bM_B + mM_M\right]\right\}}{\left\{\left(100 \cdot mM_M\right) + \left[\left(wt.\%_{M^{x+}} \cdot m \cdot \left(v_{M^{y+}} - v_{M^{x+}}\right)\right) \times \left(\frac{f_Z M_Z}{v_Z} + \frac{f_Q M_Q}{v_Q}\right)\right]\right\}} \quad (11)$$

When applied to an 36.7 BaO – 57.6 SiO_2 – 1.7 Si_3N_4 – 3.0 EuO – 1.0 Ho_2O_3 (mol.%) oxynitride glass (with 4.1 an.% of N, from ref. 69), this yields a reduced fraction in Eu^{2+} of 90.8 ± 1.8% (see Supplementary Fig. 8f). Such a significant reduction rate is expected stemming from the reductive character of oxynitride glass-forming melts, where Eu^{3+} reduction to Eu^{2+} with Si_3N_4 (which acts as a reducing agent) becomes thermodynamically feasible starting from ~1200 °C[70].

Then, in instances where three oxidation states coexist in a material, comproportionation reactions occur upon dissolution in aqueous media[35,39,40,43]. For example, in a V-bearing system, this writes:

$$V^{5+} + V^{3+} \longrightarrow 2V^{4+} \qquad (E^{\circ}_{V^{5+}/V^{4+}} > E^{\circ}_{V^{4+}/V^{3+}}) \quad (12)$$

The remaining ionic species present in solution after dissolution are strictly determined by the choice of reactive agents, in conjunction with the initial $[V^{3+}]$ to $[V^{5+}]$ ratio. The QRS method is used here as a representative case, with calculated potentiometric curves corresponding to various scenarios presented in Fig. 5a–c. Here, if $[V^{3+}] > [V^{5+}]$, then the excess of unreacted V^{3+} ions will promptly react with Fe^{3+} ions in solution as follows[43]:

$$V^{3+} + Fe^{3+} \rightarrow V^{4+} + Fe^{2+} \qquad (E^{\circ}_{Fe^{3+}/Fe^{2+}} > E^{\circ}_{V^{4+}/V^{3+}}) \quad (13)$$

In this framework, the first equivalence volume $V_{eq(1)}$ corresponds to the oxidation of the formed Fe^{2+} ions, whereas the second equivalence volume $V_{eq(2)}$ (to which $V_{eq(1)}$ is subtracted) accounts for the oxidation of the total V^{4+} ions in solution (and can be estimated based on the nominal V concentration). Although quantitative assessments of redox states cannot rely solely on these values, $V_{eq(1)}$ and $V_{eq(1)}/V_{eq(2)}$ serve as qualitative indicators of the $[V^{3+}]$ to $[V^{5+}]$ ratio, and of the $[V^{3+}]$ to total vanadium concentration ratio, respectively. As such, they are valuable tools in establishing both upper and lower concentration bounds for each species, contributing significantly to further resolving complex spectra. Assuming that the fraction of one out of the three species is known, the redox state of such intricate systems can be fully inferred. In the case of a V-bearing material where the relative concentration in $[V^{3+}]$ is known, the following

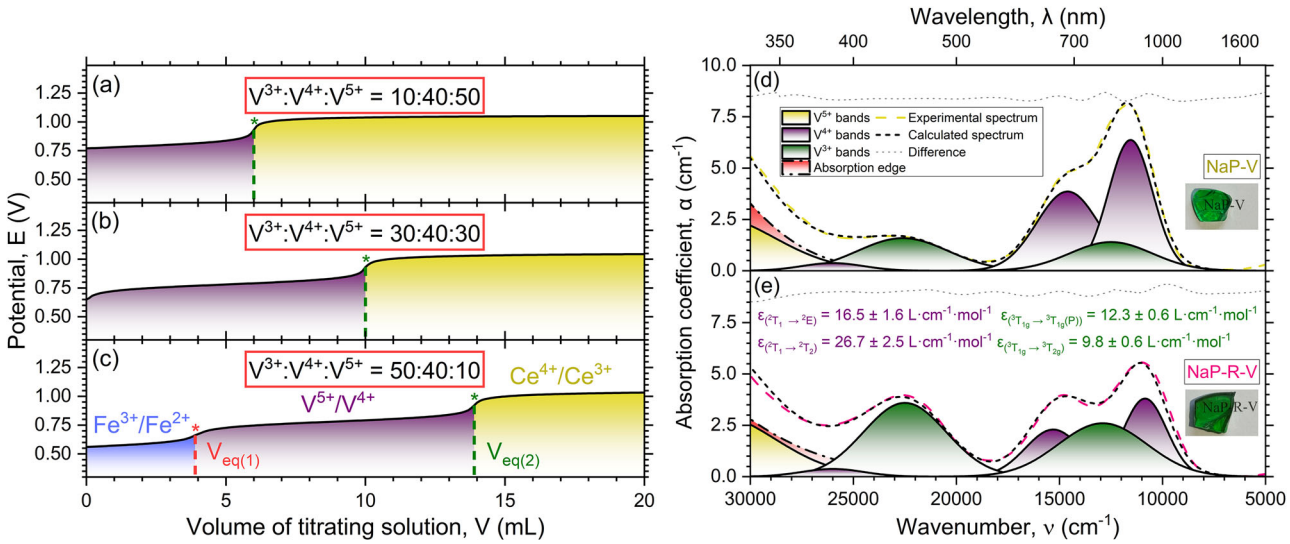

Fig. 5 | Wet-chemistry-assisted redox state quantification in systems with three coexisting oxidation states. a–c Calculated potentiometric curves considering model systems with varying initial proportions of vanadium species. The involved redox couples and their corresponding equivalence volumes are indicated. The ratio of the Ce^{4+} titrating solution to total vanadium concentration is 100. Deconvoluted optical absorption spectra of V-doped glasses synthesized **d** without a reducing agent (NaP-V), or **e** with a reducing agent (NaP-R-V). The determined molar extinction coefficients for V^{4+}- and V^{3+}-related electronic transitions are annotated. Photographs of the NaP-V and NaP-R-V samples are presented in the insets, highlighting the characteristic green color of V^{4+}- and V^{3+}-containing glasses[2].

expressions can be derived from the corresponding reaction progress table (presented in Supplementary Table 4 and detailed in Supplementary Equations 22–31):

$$f_{ox(V^{4+}/V^{3+})} = \frac{1 - 2[V3+] + V_{eq(1)}/V_{eq(2)}}{1 - [V3+] + V_{eq(1)}/V_{eq(2)}} \qquad \left([V4+] = 1 + \frac{V_{eq(1)}}{V_{eq(2)}} - 2[V3+]\right) \tag{14}$$

$$f_{ox(V^{5+}/V^{4+})} = \frac{[V3+] - V_{eq(1)}/V_{eq(2)}}{1 - [V3+]} \qquad \left([V5+] = [V3+] - \frac{V_{eq(1)}}{V_{eq(2)}}\right) \tag{15}$$

When such estimations are unavailable, or if the successive potential shifts during titration are subtle—especially at trace levels of active species—another option is using additional spectroscopic techniques. Here, the measured potentiometric curves of the NaP-V and NaP-R-V glasses are shown in Supplementary Fig. 11a, b, while their optical absorption spectra are presented in Fig. 5d, e, where the characteristic d-d electronic transitions of vanadium species are observed. The measured ε aligns with literature values ranging from 8 to 26 L cm^{-1} mol^{-1}, and the V^{3+} fraction is approximately twice as large in the reduced glass (NaP-R-V), thereby confirming the reliability of the methods[34,56,71]. Therefore, coupling wet chemistry with spectroscopic techniques simplifies data processing and interpretation, which is particularly beneficial in convoluted systems with overlapping signals or inactive species.

At last, the QOS and QRS methods are inherently non-selective and thus cannot, by themselves, be reliably applied to materials bearing multiple redox couples (e.g., Fe^{3+}/Fe^{2+} together with Mn^{3+}/Mn^{2+}), as is often the case with geologic materials or antique glasses[61,72]. Nevertheless, as previously discussed, these methods can be used to standardize more selective analytical techniques, becoming particularly valuable in complex systems involving multiple redox equilibria. A representative case is presented using three glasses with total cationic contents of 1 cat.% Fe (NaP-Fe), both 1 cat.% Fe and 1 cat.% Mn (NaP-FeMn), and 1 cat.% Mn (NaP-Mn). Their corresponding potentiometric curves and optical absorption spectra are depicted in Fig. 6a–c and Figs. 2 and 6, respectively. In the NaP-Fe sample, the characteristic Fe-related d-d electronic transitions are observed, while in the NaP-Mn sample, transitions attributed to Mn^{3+} and Mn^{2+} are evidenced, namely $^5E_g(D) \rightarrow 5T2g(D)$ at ~21,000 cm^{-1} and $6A1(S) \rightarrow 4A1(D)/4E(D)$ at ~24,000 cm^{-1}, respectively. Interestingly, the Mn^{3+}-related transition vanishes entirely in the NaP-FeMn spectrum, accompanied by a marked decrease in the intensity of the Fe^{2+}-related bands. In fact, oxidized fractions determined via the QOS method yield values of 82.2 ± 1.6% for the NaP-Fe sample and 5.8 ± 0.1% for the NaP-Mn glass. From these two insights, molar extinction coefficients are achieved: $\varepsilon(^5E_g(D) \rightarrow {}^5T_{2g}(D)) = 22 \pm 1$ L cm^{-1} mol^{-1} and $\varepsilon(6A1(S) \rightarrow 4A1(D)/4E(D)) = 0.09 \pm 0.01$ L cm^{-1} mol^{-1}, which fall in the (particularly wide) range of ε reported in the literature, extending from 20 to 135 L cm^{-1} mol^{-1} and from 0.04 to 0.5 L cm^{-1} mol^{-1}, respectively[2,27,61,62]. By reinjecting the acquired ε into the collected NaP-FeMn spectrum, an oxidized fraction of 86.6 ± 2.5% is derived for the Fe^{3+}/Fe^{2+} couple. From this, it becomes evident that Mn^{3+} and Fe^{2+} stoichiometrically react until completion in the glass-forming melt, following:

$$Mn^{3+} + Fe^{2+} \rightarrow Mn^{2+} + Fe^{3+} \qquad (E^{\circ}_{Mn^{3+}/Mn^{2+}} > E^{\circ}_{Fe^{3+}/Fe^{2+}}) \tag{16}$$

Although such a methodology necessitates preliminary determinations using single redox systems of comparable compositions, it proves decisive in preventing any misestimation of the active species of interest, while allowing for the calibration and subsequent probing of environment-dependent redox reactions and equilibria within glass-forming melts and associated media.

Discussion

Two wet-chemical techniques for quantifying the redox state of materials were developed and subsequently validated utilizing analytical standards from diverse chemical systems, encompassing both oxidizing and reductive species. Utilizing simple, portable instrumentation and nontoxic, readily available reagents, these methods demonstrated high precision and versatility across a broad range of host compositions, crystallization rates, and redox couples. Their reliability was corroborated through concordance with complementary analytical techniques, yielding a robust dataset valuable for advancements, particularly in glass science.

Despite being destructive, the minimal reagent and sample quantities required (typically tens to hundreds of milligrams) render the techniques well-suited for laboratory-scale investigations. Their procedural simplicity, which obviates the need for preparatory steps (cutting, polishing, sputter

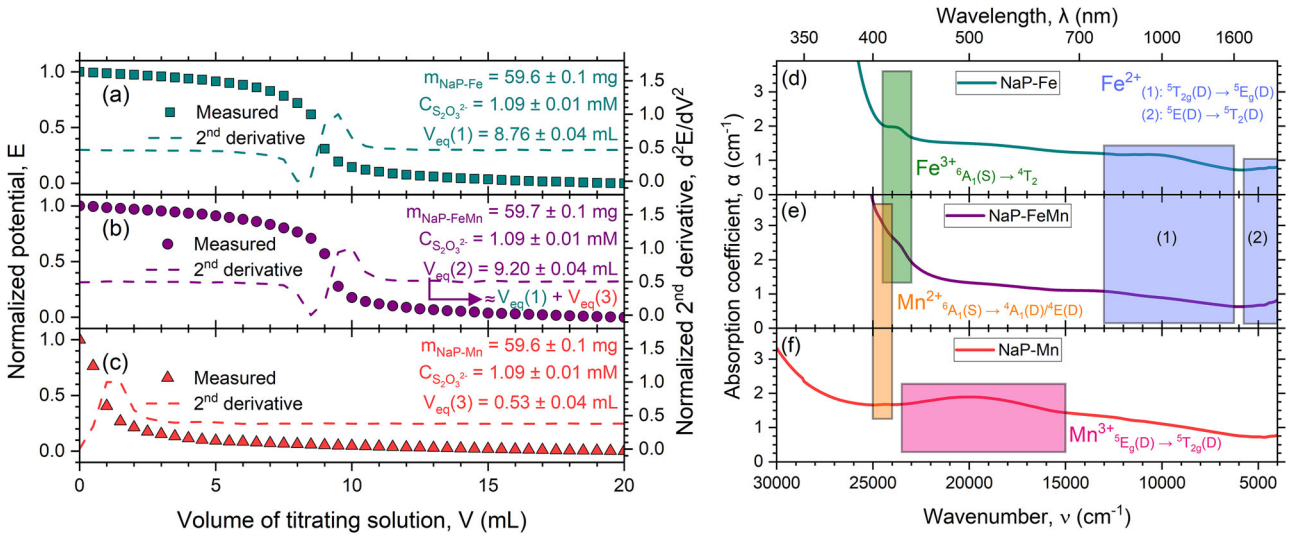

Fig. 6 | Wet-chemistry-assisted redox state quantification in systems with mixed redox couples. Normalized potentiometric curves and associated second derivatives during the titration of NaP glasses doped with **a** 1 cat.% of Fe (NaP-Fe), **b** 1 cat.% of Fe and 1 cat.% of Mn (NaP-FeMn), and **c** 1 cat.% of Mn (NaP-Mn). While the titration curve of the NaP-Mn sample is shown alongside those of the NaP-Fe and NaP-FeMn samples under comparable experimental conditions, its exact oxidized fraction was determined independently in an additional experiment to ensure a well-resolved equivalence volume. Optical absorption spectra of **d** NaP-Fe, **e** NaP-FeMn, and **f** NaP-Mn. Fe^{3+}-, Fe^{2+}-, Mn^{3+}-, and Mn^{2+}-related electronic transitions are highlighted. Slight deviations at small wavenumbers are ascribed to residual water. Photographs of the NaP-Fe, NaP-FeMn, and NaP-Mn samples are presented in the insets, highlighting the characteristic yellow, light orange, and purple colors of Fe^{3+}-, Mn^{2+}-, and Mn^{3+}-containing glasses, respectively[2,61].

coating), combined with the rapid determination of equivalence volumes via potentiometry or colorimetry, positions them as promising candidates for high-throughput implementation through automation using integrated absorption spectroscopy or potentiometric systems. In addition to redox quantification, the methods offer environmentally relevant applications, including the passivation of hazardous species (Cr^{6+}) and the selective recovery of raw materials through sequential pH-controlled precipitation.

The Quantification of Oxidizing Species (QOS) and Quantification of Reductive Species (QRS) methods provide considerable value in spatially and energetically resolved spectroscopic techniques by addressing redox state misestimations and improving signal interpretation through standardization. This, in turn, facilitates deeper investigations into the local structures of polyvalent cations, an area of ongoing scientific debate and interest. These methods are particularly relevant for studies involving off-stoichiometry materials such as glasses, thin films, or doped crystals, where the interplay between complex chemical composition, structure, and material properties is often non-linear and difficult to predict. In these systems, even minor changes in redox state—and the resulting changes in local structure and induced vacancies—can substantially alter charge carrier mobility and trapping dynamics. Such insights are crucial for advancing the understanding of complex phenomena and the corresponding mechanisms (photoinduced conductivity, persistent luminescence).

In essence, integrating precisely defined redox states within material design can further enhance their tunability, enabling access to exceptional properties and unique features through combined control over the redox state, crystallization architecture, and defect distribution and concentration. These approaches find broad applicability across material science research and applications, ranging from tailored surface and bulk properties to high stimulus responsiveness and introduced functionalities.

Methods

Sample preparation

Four series of glass compositions encompassing broad ranges in silica content (up to 66.7 mol.%), optical basicities (from $\Lambda_{th} = 0.52$ to $\Lambda_{th} = 0.73$), synthesis temperatures (from 1100 to 1600 °C), and high dopant solubility limits (up to 10 cat.%), were selected. Their formulations, optical basicities, and corresponding investigated dopants and doping ranges are summarized in Supplementary Table 2. A supplementary glass series, NaP-R, was considered to examine the consequences of reducing conditions by introducing an excess amount of sugar as a reducing agent, equivalent to twice the stoichiometric amount for complete dopant reduction. Each series was doped with different concentrations of dopants while maintaining the original cationic ratios of the parent glass (e.g., Na/P = 1 for doped NaP glasses), except for the LS series where the dopants stoichiometrically substitute for Si. Glass batches were prepared from analytical grade raw materials: Na_2CO_3 (Carl Roth, 99.5%), $(NH_4)_2HPO_4$ (Carl Roth, 97%), Li_2CO_3 (Chemapol, 99.5%), SiO_2 (Reachim, 96%), H_3BO_3 (Merck, 99%), $CaCO_3$ (Merck, 99%), Al_2O_3 (Pengda Munich, 99.99%), MgO (Acros, 97%), Cs_2CO_3 (Fluka, 98%), $BaCO_3$ (Merck, 99.9%), TiO_2 (VK labor, 99%), Cr_2O_3 (Laborchemie Apolda, 99%), MnO (Aldrich, 99%), $CoCO_3$ (VK labor, 99%), CuO (HB labor, 99%), Nb_2O_5 (РЕАХИМ, 99%), MoO_3 (Reachim, 99%), SnO_2 (VEB Berlin-Chemie, 99%), Eu_2O_3 (Projector, 99.999%), Yb_2O_3 (Projector, 99.99%), WO_3 (Bergbau und Hütten, 99%), and Bi_2O_3 (Merck, 99%). Appropriate quantities of each reagent were thoroughly weighed and mixed to ensure proper homogeneity. For the LS and CAS series, the batches were first calcined at 1000 °C for 6 h to facilitate complete gas release. The obtained mixtures were then melted in Pt-Rh crucibles at 1400 and 1600 °C for 1 h (air atmosphere), respectively. A subsequent 0.5 h homogenization step was applied under identical conditions post-casting. In the case of the NaP and NaB series, the mixed starting materials were melted in alumina crucibles at 1100 °C for 1 h (air atmosphere) to ensure homogeneity while preventing elemental losses. The resulting melts were ultimately cast into carbon molds, or splat-quenched between copper plates for large dopant concentrations (>2 cat.%) before final annealing at 400 °C (LS series) or 750 °C (CAS series), and subsequently stored in a desiccator. Moreover, glass compositions reported in recent works—where either (i) the redox state was characterized by XANES spectroscopy (a Ce-doped aluminosilicate glass)[18], or (ii) elements in uncommon oxidation states were evidenced (e.g., Mn^{5+} and Mn^{6+} in the 32 B_2O_3 – 68 Na_2O and 50 SiO_2 – 50 Cs_2O – 10 BaO chemical systems, respectively)—were also prepared, employing identical experimental conditions[27,50].

Physical characterization

X-ray diffraction (XRD) measurements were performed on powdered glass samples to ensure their amorphousness using a Rigaku Miniflex 600 diffractometer with CuK_α radiation (1.54056 Å) in the 5–80° 2θ range with a 5° mm^{-1} scan speed.

Differential scanning calorimetry (DSC) measurements were carried out using a Netzsch STA 449 F3 Jupiter instrument to define the annealing temperatures. Bulk samples were loaded in a platinum crucible, and subsequently heated under N_2 flow with a heating rate of 10 K min^{-1}.

The specimen density was determined by the Archimedes method at 25 °C utilizing ethanol as the solvent ($\rho = 0.78806$ g cm^{-3}).

Optical absorption spectra were collected in the 200–3000 nm range using a double-beam UV-Vis-NIR spectrophotometer (Agilent Cary 5000), and specimens preliminarily polished to optical-grade quality.

Redox state quantification

As furnished KI (VK labor, 99.5%), $(NH_4)_2Fe(SO_4)_2{\cdot}6H_2O$ (Merck, 99%), $Na_2S_2O_3{\cdot}5H_2O$ (Merck, 99.5%), starch (Chemapol, 99%), Fe_2O_3 (Aldrich, 99%), $Ce(SO_4)_2{\cdot}4H_2O$ (Laborchemie Apolda, 99.8%), $Sr_{0.95}Eu_{0.02}Dy_{0.03}Al_2O_4$ (Aldrich, 99%), borofloat® 33 glass doped with 15 ppm Fe (Schott AG, Jena, Germany), and 0.025 M ferroin (Thermo Scientific) raw materials were used, along with 12 M HCl (Carl Roth) and 18 M H_2SO_4 (Carl Roth) acids. Analytical standards included: TiN (Johnson Matthey, 99%), V_2O_5 (Merck, 99%), MnO_2 (Riedel-de Haën, 95%), Fe_3O_4 (VK labor, 99%), FeS (Thermo Scientific, 99.9%), Co_3O_4 (VK labor, 99%), Cu_2O (Aldrich, 97%), Cu_2S (Thermo Scientific, 99.5%), SnF_2 (Aldrich, 99%), CeO_2 (Projector, 99.99%), Pr_6O_{11} (Projector, 99.99%), and Tb_4O_7 (Projector, 99.99%). Materials elaborated in previous studies were also used, including a $Ba_{3.5}Eu_{0.3}Ho_{0.2}Si_6O_{15.5}$ phosphor, and a 36.7 BaO – 57.6 SiO_2 – 1.7 Si_3N_4 – 3.0 EuO – 1.0 Ho_2O_3 glass[52,69]. All experimental procedures were conducted under a fume hood, using iron-free borosilicate glassware and distilled water. Considering instances involving extremely low amounts of active species (tens of ppm) and correspondingly very dilute titrating solutions, the use of chemically inert containers (e.g., Teflon) is recommended to minimize contamination during the dissolution steps. It should be noted, however, that in such dilute media, longer equilibration times are required during titration after each incremental addition of titrant to achieve complete reaction of the analyte. This behavior arises from the nature of the reaction (non-zero order) and the associated kinetics, as exemplified in Supplementary Fig. 12a–d for borofloat® 33 glass doped with 15 ppm of Fe, analyzed using the QRS method. To achieve rapid yet precise titrations under optimum conditions, a titrant concentration of no less than 10^{-3} M should thus be employed, ideally with small analyte volumes ranging from 50 to 350 mL, in conjunction with suitable indicators (e.g., starch, ferroin). To prevent concentration variations due to prolonged storage, all solutions were freshly prepared on the day of each experiment. Hydrochloric acid was chosen over other inorganic acids to ensure quick sample dissolution at high temperatures while avoiding undesired redox (HNO_3, H_2SO_4) or precipitation (HF) reactions. For silica-rich samples, residual undissolved SiO_2 particles led to slightly cloudy solutions, though this had no consequences on the equivalence volume determinations[46]. Potential measurements were carried out using an epoxy body Redox/ORP Sure Flow 9678BNWP combined electrode (Pt indicator electrode with Ag/AgCl reference) connected to an Orion Star A211 pH meter (Thermo Scientific). The use of a potentiometer was deemed preferable for ensuring the most precise equivalence volume measurements and, consequently, the most accurate oxidized fraction assessments. Analytical uncertainties were typically within 2–3% of the determined measurand. The aqueous waste generated per analyzed sample ranged from 200 to 500 mL, comparable to existing methods that require complete sample dissolution prior to quantifying a multivalent element (e.g., EPA Method 3060 A, as well as ISO standards 4298:2022 and 9035:1989 for Cr, Mn, and Fe species, respectively), where total waste—including the volumes involved in sample dissolution, solution dilution, pH adjustments, and titrant preparation—typically amounts from 400 to 600 mL per sample. A calculation sheet (Supplementary Data 1) and a work flow chart are provided in the Supplementary Information for conducting the experiments systematically (see Supplementary Fig. 1). Every oxidized fraction measured in the present work is compiled in Supplementary Table 3.

A typical experiment using the QOS method, with representative masses and concentrations provided in brackets, is described as follows: A minimal quantity of a finely ground specimen (15–150 mg) was carefully weighed into an Erlenmeyer flask to ensure an appreciable equivalence volume near 10 mL while facilitating rapid dissolution and minimizing volume blanks. An appropriate amount of KI—corresponding to 20 times the quantity required to fully reduce the active species (0.05–2 g)—was dissolved in 20 mL of distilled water and added to the flask. Following the addition of 10 mL of concentrated hydrochloric acid, the solution was quickly connected to a reflux condenser, subsequently immersed in a preheated silicone oil bath at 100 °C, and stirred until complete dissolution. This step generally required ~10 min, even in the presence of small concentrations of active species (and thus larger sample masses) within chemically durable, silica-rich matrices, as evidenced by the sample mass (m_{sample}) and dissolution time (t_{diss}) invariance of the determined oxidized fractions (see Supplementary Fig. 9a, b). Any iodine adhering to the condenser walls was rinsed, after which the solution was quickly transferred to a beaker and diluted to 350 mL to quench the reaction. Titration was performed using a $Na_2S_2O_3{\cdot}5H_2O$ solution (0.002–0.05 M), with the equivalence volume determined via (i) potentiometry, by identifying the inflection point, and (ii) colorimetry, by observing the color change from yellow to colorless (consumption of I_2). Alternatively, to enhance endpoint visualization, 0.5 mL of a 0.01 g mL^{-1} starch solution can be added near the equivalence point, causing the solution to shift from deep blue to colorless. A blank was systematically performed using identical volumes and heating conditions to account for the oxidation of I- ions; the corresponding equivalence volume (~0.5 mL, also determined from the dependence of the equivalence volume on the introduced sample mass and validated by the invariance of the derived oxidized fractions, to account for any potential matrix effects notably at low concentrations, as shown in Supplementary Fig. 3a–c) was subtracted from the measured value for the sample. In the absence of prior estimation of the oxidized fraction, the KI amount was initially determined assuming complete oxidation ($f_{ox} = 100\%$). This amount was then refined in a second experiment by incorporating the first experimental estimate of the oxidized fraction. In instances involving small concentrations of active species—and thus where the equivalence volume approached that of the blank—masses, concentrations, and dissolution time were adjusted accordingly to achieve larger, more appreciable equivalence volumes (e.g., by diluting to 50 mL instead). Note that quantifying the fraction of oxidizing species through back titration of the remaining reactive agent—such as Fe^{2+} in cerimetry—was found unsuitable, as it involved limited excess in reactive agent and thus introduced competition in reactivity with Cl^- ions.

The QRS method follows a similar protocol but incorporates an additional preliminary step. Specifically, an excess of Fe^{3+}—introduced as Fe_2O_3, corresponding to 20 times the quantity required to fully oxidize the active species (0.005–0.1 g)—was first dissolved independently. In the absence of prior estimation of the reduced fraction, the Fe_2O_3 amount was determined assuming complete reduction ($f_{red} = 100\%$). This was achieved by adding 10 mL of concentrated hydrochloric acid to an Erlenmeyer flask, connecting it to a reflux condenser, immersing the mixture in a preheated silicone oil bath at 100 °C, and stirring until complete dissolution. For redox couples with a standard potential smaller than 0 V (e.g., Eu^{3+}/Eu^{2+}, Nb^{5+}/Nb^{4+}), an excess of Fe^{3+} corresponding to 100 times the quantity required to fully oxidize the active species was employed to prevent any side reaction. Following dissolution, the solution was removed from the apparatus, and a minimal quantity of a finely ground specimen (5–150 mg) was carefully weighed and introduced into the flask to ensure an appreciable equivalence volume near 10 mL while facilitating rapid dissolution and minimizing volume blanks. The solution was then subjected to heating and stirring at 100 °C. This step generally required ~10 min, even in the presence of small

concentrations of active species (and thus larger sample masses) within chemically durable, silica-rich matrices, as evidenced by the sample mass and dissolution time invariance of the determined reduced fractions (see Supplementary Fig. 9a, b). Subsequently, it was transferred to a beaker and diluted to 350 mL. Titration was performed using a $Ce(SO_4)_2{\cdot}4H_2O$ solution (0.001–0.01 M, dissolved in a 1 M solution of sulfuric acid to avoid the evolution of Cl_2 gas), with the equivalence volume determined via (i) potentiometry, by identifying the inflection point, and (ii) colorimetry, by observing the color change from colorless (or pale yellow) to deep yellow (excess of Ce^{4+}). For improved endpoint detection, both by potentiometry and by colorimetry, a small quantity of ferroin—corresponding in moles to 0.5 mL of the titrating solution, and subsequently subtracted from the final equivalence volume—can be added, causing the solution to shift from deep red to cyan ($[Fe(o\text{-phen})_3]^{2+}$ to excess of $[Fe(o\text{-phen})_3]^{3+}$). Blanks were required exclusively for long experiments (>1 h) involving samples with substantial resistance to dissolution (i.e., the blank volumes approached the experimental error for short dissolution times, as presented in Supplementary Fig. 3d–f). In such rare instances, they were performed using comparable initial amounts of ferrous ions–introduced as $(NH_4)_2Fe(SO_4)_2{\cdot}6H_2O$—under identical volumes and heating conditions, to account for the oxidation of Fe^{2+} ions; the corresponding difference in equivalence volume was subtracted from the measured value for the sample.

Data availability

All data supporting the findings in this study are available within this Article and its Supplementary Information. Source data for all main figures are provided with this paper. Any additional data are available from the corresponding author upon request.

Received: 22 December 2025; Accepted: 5 February 2026;
Published online: 21 March 2026

References

1. Di Genova, D., Vasseur, J., Hess, K. U., Neuville, D. R. & Dingwell, D. B. Effect of oxygen fugacity on the glass transition, viscosity and structure of silica- and iron-rich magmatic melts. *J. Non Cryst. Solids* **470**, 78–85 (2017).
2. De Ligny, D. & Möncke, D. *Colors in Glasses*. *Springer Handbooks*. in Springer Handbook of Glass (eds Musgraves, J.D., Hu, J. & Calvez, L.) (Springer, 2019).
3. Jeoung, J., Poisl, W. H., Weinberg, M. C., Smith, G. L. & Li, H. Effect of oxidation state of iron on phase separation in sodium silicate glasses. *J. Am. Ceram. Soc.* **84**, 1859–1864 (2001).
4. Van den Eeckhout, K., Smet, P. F. & Poelman, D. Persistent luminescence in Eu^{2+}-doped compounds: a review. *Materials* **3**, 2536–2566 (2010).
5. Gao, G. et al. Faraday Rotation and photoluminescence in heavily Tb^{3+}-doped GeO_2-B_2O_3-Al_2O_3-Ga_2O_3 glasses for fiber-integrated magneto-optics. *Sci. Rep.* **5**, 1–6 (2015).
6. Chen, K. et al. A facile approach for generating ordered oxygen vacancies in metal oxides. *Nat. Mater*. 1–8 https://doi.org/10.1038/s41563-025-02171-4 (2025).
7. Schreiber, H. D. *The Characterization of Individual Redox Ions in Glasses*. (eds Ross. D.R., Condrate, R.A., Snyder, R.L.) vol **15**, (647–658) (Springer, 1983).
8. Lerner, A. H. et al. Improving the reliability of Fe- and S-XANES measurements in silicate glasses: correcting beam damage and identifying Fe-oxide nanolites in hydrous and anhydrous melt inclusions. *Chem. Geol.* **586**, 120610 (2021).
9. Neuville, D. R., Cicconi, M. R. & Losq, C. Le. How to Measure the Oxidation State of Multivalent Elements in Minerals, Glasses, and Melts? *Magma Redox Geochemistry* 257–281 https://doi.org/10.1002/9781119473206.ch13 (2021).
10. Smythe, D. J., Brenan, J. M., Bennett, N. R., Regier, T. & Henderson, G. S. Quantitative determination of cerium oxidation states in alkali-aluminosilicate glasses using M4,5-edge XANES. *J. Non Cryst. Solids* **378**, 258–264 (2013).
11. Austin, I. G. & Mott, N. F. Polarons in crystalline and non-crystalline materials. *Adv. Phys.* **50**, 757–812 (2001).
12. Génois, R., Jobic, S., Ouvrard, G., Massuyeau, F. & Gautier, R. The crucial impact of cerium reduction on photoluminescence. *Appl. Mater. Today* **20**, 100643 (2020).
13. Li, H., Li, W., Gu, S., Wang, F. & Zhou, H. In-Built Tb^{4+}/Tb^{3+} redox centers in terbium-doped bismuth molybdate nanograss for enhanced photocatalytic activity. *Catal. Sci. Technol.* **6**, 3510–3519 (2016).
14. Feng, A. & Smet, P. F. A review of mechanoluminescence in inorganic solids: compounds, mechanisms, models and applications. *Materials* **11**, 484 (2018).
15. Berry, A. J. & O'Neill, H. S. C. A XANES determination of the oxidation state of chromium in silicate glasses. *Am. Mineral.* **89**, 790–798 (2004).
16. Miller, L. A., O'Neill, H. S. C., Berry, A. J. & Glover, C. J. The oxidation state and coordination environment of antimony in silicate glasses. *Chem. Geol.* **524**, 283–294 (2019).
17. Ebendorff-Heidepriem, H. & Ehrt, D. Formation and UV absorption of cerium, europium and terbium ions in different valencies in glasses. *Opt. Mater.* **15**, 7–25 (2000).
18. Donatini, A., Georges, P., Fevre, T., Cormier, L. & Neuville, D. R. Investigating Cerium redox changes between aluminosilicate glass and melt: a multispectroscopic approach. *J. Chem. Phys*. **160**, 124503 (2024).
19. Zandonà, A. et al. Effect of the interaction between basicity and reductive character of melting atmosphere—both extreme—on the oxidation and coordination states assumed by transition metals when doped to silicate glasses. *J. Non. Cryst. Solids* **637**, 123038 (2024).
20. Kido, L., Müller, M. & Rüssel, C. Evidence of redox relaxation during thermal treatment of soda lime silica glasses doped with chromium and manganese. *Chem. Mater.* **17**, 3929–3934 (2005).
21. Duffy, J. A. A review of optical basicity and its applications to oxidic systems. *Geochim. Cosmochim. Acta* **57**, 3961–3970 (1993).
22. Duffy, J. A. Redox equilibria in glass. *J. Non Cryst. Solids* **196**, 45–50 (1996).
23. Rodriguez, C. P., McCloy, J. S., Schweiger, M. J., Crum, J. V. & Winschell, A. Optical Basicity and Nepheline Crystallization in High Alumina Glasses. in *Pacific Northwest National Laboratory (PNNL-20184)* (Richland, 2011).
24. Dimitrov, V. & Sakka, S. Electronic oxide polarizability and optical basicity of simple oxides. *I. J. Appl. Phys.* **79**, 1736–1740 (1996).
25. Zhao, X., Wang, X., Lin, H. & Wang, Z. Electronic polarizability and optical basicity of lanthanide oxides. *Phys. B Condens. Matter* **392**, 132–136 (2007).
26. Duffy, J. A. Polarisability and polarising power of rare earth ions in glass: an optical basicity assessment. *Phys. Chem. Glas.* **46**, 1–6 (2005).
27. Ashjari, A. et al. Unusually high oxidation states of manganese in high optical basicity silicate glasses. *Opt. Mater. X* **24**, 100371 (2024).
28. Heß, L. Unusual High Oxidation States of d-Transition Metal Ions in Glasses. in *Bachelor Thesis* (Ger. Friedrich Schiller Univ. Jena, 2015).
29. Burnham, A. D. et al. The oxidation state of europium in silicate melts as a function of oxygen fugacity, composition and temperature. *Chem. Geol.* **411**, 248–259 (2015).
30. Pinet, O., Phalippou, J. & Di Nardo, C. Modeling the redox equilibrium of the Ce^{4+}/Ce^{3+} couple in silicate glass by voltammetry. *J. Non Cryst. Solids* **352**, 5382–5390 (2006).
31. Farah, H. Optical basicity analysis of vanadium-bearing silicate glasses/melts. *J. Am. Ceram. Soc.* **91**, 3915–3919 (2008).
32. Gütlich, P., Schröder, C. & Schünemann, V. Mössbauer spectroscopy—an indispensable tool in solid state research. *Spectrosc. Eur.* **24**, 21–32 (2012).

33. Mekki, A., Ziq, K. A., Holland, D. & McConville, C. F. Magnetic properties of praseodymium ions in Na_2O-Pr_2O_3-SiO_2 glasses. *J. Magn. Magn. Mater.* **260**, 60–69 (2003).
34. Leister, M. et al. Redox states and coordination of vanadium in sodium silicates melted at high temperatures. *Phys. Chem. Glas.* **40**, 319–325 (1999).
35. Johnston, W. D. Oxidation-reduction equilibria in molten $Na_2O{\cdot}SiO_2$ glass. *J. Am. Ceram. Soc.* **48**, 184–190 (1964).
36. Schreiber, H. D. et al. Compositional dependence of redox equilibria in sodium silicate glasses. *J. Non Cryst. Solids* **177**, 340–346 (1994).
37. Schuessler, J. A., Botcharnikov, R. E., Behrens, H., Misiti, V. & Freda, C. Oxidation state of iron in hydrous phono-tephritic melts. *Am. Mineral.* **93**, 1493–1504 (2008).
38. Morsi, M. M., Metwalli, E. E. D. S. & Mohamed, A. A. Modified chemical method for determination of Cu^+ ions in some cu containing phosphate glasses and effect of composition on the Cu^{2+}/Cu(tot) ratio. *Phys. Chem. Glas.* **40**, 314–318 (1999).
39. Schreiber, H. D. An electrochemical series of redox couples in silicate melts: a review and applications to geochemistry. *J. Geophys. Res. Solid Earth* **92**, 9225–9232 (1987).
40. Mittelstadt, R. & Schwerdtfeger, K. The dependence of the oxidation state of vanadium on the oxygen pressure in melts of VO_x, Na_2O-VO_x, and CaO-SiO_2-VO_x. *Metall. Trans. B* **21**, 111–120 (1990).
41. Barthauer, G. L. & Pearce, D. W. Analytical chemistry of the rare earths. the active-oxygen determination. *Ind. Eng. Chem. Anal. Ed.* **18**, 479–480 (1946).
42. Serhan, M. et al. The chemical and physical properties of tetravalent lanthanides: Pr, Nd, Tb, and Dy. *Dalt. Trans.* **49**, 15945–15987 (2020).
43. Bratsch, S. G. Standard electrode potentials and temperature coefficients in water at 298. *15 K. J. Phys. Chem. Ref. Data* **18**, 1–21 (1989).
44. Haynes, W. M. *CRC Handbook of Chemistry and Physics*. 95th edn (CRC Press, 2015).
45. Sroor, F. M. A. & Edelmann, F. T. Tetravalent chemistry: inorganic. *Rare Earth Elem. Fundam. Appl*. 313–320 https://doi.org/10.1002/9781119951438.eibc2033 (2012).
46. Pourbaix, M. *Atlas of Electrochemical Equilibria in Aqueous Solutions*. Vol. 1 Pergamon Press, (1966).
47. Kim, S. W., Shimoyama, T. & Hosono, H. Solvated electrons in high-temperature melts and glasses of the room-temperature stable electride $[Ca_{24}Al_{28}O_{64}]^{4+}.4e^-$. *Science* **333**, 71–74 (2011).
48. Kim, H. S. et al. Oxygen vacancies enhance pseudocapacitive charge storage properties of MoO_{3-x}. *Nat. Mater.* **16**, 454–462 (2017).
49. Wang, J., Mueller, D. N. & Crumlin, E. J. Recommended strategies for quantifying oxygen vacancies with X-ray photoelectron spectroscopy. *J. Eur. Ceram. Soc.* **44**, 116709 (2024).
50. Zandonà, A. et al. Oxidation and coordination states assumed by transition metal dopants in an invert ultrabasic silicate glass. *J. Non. Cryst. Solids* **603**, 122094 (2023).
51. Piotrowski, W. M. et al. Mn^{5+} lifetime-based thermal imaging in the optical transparency windows through skin-mimicking tissue phantom. *Adv. Opt. Mater.* **11**, 2202366 (2023).
52. Duval, A., Suffren, Y., Benabdesselam, M., Houizot, P. & Rouxel, T. Luminescence and mechanoluminescence of $Ba_4Si_6O_{16}$:Eu^{2+}, RE phosphors. *J. Chem. Phys.* **159**, 134501 (2023).
53. Clabau, F. et al. Fluorescence and phosphorescence properties of the low temperature forms of the $MAl_2Si_2O_8$:Eu^{2+} (M=Ca, Sr, Ba) compounds. *J. Solid State Chem.* **181**, 1456–1461 (2008).
54. Clabau, F. Phosphorescence: Mécanismes et Nouveaux Matériaux. *PhD Thesis, Univ. Nantes* (2005).
55. Ehrt, D., Leister, M. & Matthai, A. Redox behaviour in glass forming melts. *Molten Salt Forum* **5–6**, 547–554 (1998).
56. Ehrt, D., Leister, M., Matthai, C., Russel, C. C. & Breitbarth, F. Determination of the redox states of vanadium in glasses and melts by different methods. *Fundam. Glas. Sci. Technol. Conf.* **204**, 211 (1997).
57. Ehrt, D., Leister, M. & Matthai, A. Polyvalent elements iron, tin and titanium in silicate, phosphate and fluoride glasses and melts. *Phys. Chem. Glas.* **42**, 231–239 (2001).
58. Rossel, C. The Electrochemical behavior of some polyvalent elements in a soda-lime-silica glass melt. *J. Non Cryst. Solids* **119**, 303–309 (1990).
59. Möncke, D. Photo-ionization of 3d-ions in fluoride-phosphate glasses. *Int. J. Appl. Glas. Sci.* **6**, 249–267 (2015).
60. Sycheva, G. A. & Grishchenko, L. V. Specific features of the glass formation in the R_2O–B_2O_3, R_2O–SiO_2, and R_2O–B_2O_3–SiO_2 (R = Rb, Cs) systems. *Glas. Phys. Chem.* **34**, 260–264 (2008).
61. Möncke, D., Papageorgiou, M., Winterstein-Beckmann, A. & Zacharias, N. Roman glasses coloured by dissolved transition metal ions: redox-reactions, optical spectroscopy and ligand field theory. *J. Archaeol. Sci.* **46**, 23–36 (2014).
62. Möncke, D., Sirotkin, S., Stavrou, E., Kamitsos, E. I. & Wondraczek, L. Partitioning and structural role of Mn and Fe ions in ionic sulfophosphate glasses. *J. Chem. Phys*. **141**, 224509 (2014).
63. Hirayama, C., Castle, J. G. & Kuriyama, M. Spectra of iron in alkaline earth phosphate glasses. *Phys. Chem. Glas.* **9**, 109 (1968).
64. Ceglia, A. et al. Iron speciation in soda-lime-silica glass: a comparison of XANES and UV-vis-NIR spectroscopy. *J. Anal. Spectrom.* **30**, 1552–1561 (2015).
65. Volotinen, T. T., Parker, J. M. & Bingham, P. A. Concentrations and site partitioning of Fe^{2+} and Fe^{3+} ions in a soda-lime-silica glass obtained by optical absorbance spectroscopy. *Phys. Chem. Glas. Eur. J. Glas. Sci. Technol. Part B* **49**, 258–270 (2008).
66. Bingham, P. A., Parker, J. M., Searle, T., Williams, J. M. & Fyles, K. Redox and clustering of iron in silicate glasses. *J. Non Cryst. Solids* **253**, 203–209 (1999).
67. Ehrt, D., Carl, M., Kittel, T., Müller, M. & Seeber, W. High-performance glass for the deep ultraviolet range. *J. Non Cryst. Solids* **177**, 405–419 (1994).
68. Schreurs, J. W. H. & Brill, R. H. Iron and sulfur related colors in ancient glasses. *Archaeometry* **26**, 199–209 (1984).
69. Duval, A., Houizot, P., Rocquefelte, X. & Rouxel, T. Mechanoluminescence of (Eu, Ho)-doped oxynitride glass-ceramics from the BaO-SiO_2-Si_3N_4 chemical system. *Appl. Phys. Lett.* **123**, 011905 (2023).
70. Duval, A., Houizot, P. & Rouxel, T. Review: elaboration, structure, and mechanical properties of oxynitride glasses. *J. Am. Ceram. Soc.* **106**, 1611–1637 (2022).
71. Cicconi, M. R. et al. Influence of vanadium on optical and mechanical properties of aluminosilicate glasses. *Front. Mater.* **7**, 1–17 (2020).
72. Hirschmann, M. M. Magma oceans, iron and chromium redox, and the origin of comparatively oxidized planetary mantles. *Geochim. Cosmochim. Acta* **328**, 221–241 (2022).
73. Morss, L. R. Thermochemical properties of yttrium, lanthanum, and the lanthanide elements and ions. *Chem. Rev.* **76**, 827–841 (1976).

Acknowledgements

We acknowledge financial support from the Carl Zeiss Foundation (Durchbrüche 2019).

Author contributions

A.D. conceived the idea. L.W. provided funding and resources. A.D. and F.S. synthesized and polished the materials. N.G.-M. performed X-ray diffraction and DSC determinations. A.D. collected and analyzed optical absorption spectra. A.D., N.G.-M., and O.S. tested and validated the methodology. A.D. conducted the titrations. A.D., F.S., O.S., and L.W. analyzed and interpreted the data and wrote and revised the manuscript. All authors added and commented on the manuscript and its revisions.

Funding

Open Access funding enabled and organized by Projekt DEAL.

Competing interests
The authors declare no competing interests.

Additional information
Supplementary information The online version contains supplementary material available at https://doi.org/10.1038/s43246-026-01109-w.

Correspondence and requests for materials should be addressed to Alexis Duval or Lothar Wondraczek.

Peer review information *Communications Materials* thanks the anonymous reviewers for their contribution to the peer review of this work. A peer review file is available.